Reduction Kinetics of La Modified NiO/La-γAl_2O_3 Oxygen Carrier for Chemical-Looping Combustion

Mohammad M. Hossain,[†] Mohammad R. Quddus,[‡] and Hugo I. de Lasa*[,‡]

Department of Chemical Engineering, King Fahd University of Petroleum & Minerals, Dhahran 31261, Saudi Arabia, and Chemical Reactor Engineering Center, Department of Chemical and Biochemical Engineering, The University of Western Ontario, London, ON, Canada N6A 5B9

La modified Ni/La-γAl_2O_3 oxygen carrier reduction kinetics is investigated using temperature programmed reduction (TPR) and a parameter nonlinear regression analysis. TPR profile study and XRD analysis of the completely oxidized samples show that NiO is the prevalent phase of the oxygen carrier. Hydrogen pulse chemisorption demonstrates that the nickel crystallite sizes remain unchanged over repeated reduction/oxidation cycles. A nucleation and nuclei growth model and an unreacted shrinking core model are developed based on the oxygen carrier characterization. Model discrimination is conducted based on SSQ, goodness of fittings, and minimum cross-correlation coefficients. On the basis of these statistical indicators, it is established that the random nucleation model describes the reduction of the oxygen carrier adequately. The estimated value of the activation energy for the La modified Ni/La-γAl_2O_3 sample is found to be 73.4 ± 2.6 kJ/mol, with this being significantly lower than the activation energy for the unmodified Ni/γAl_2O_3 sample (104.5 ± 3 kJ/mol). This suggests that the unmodified oxygen carrier requires higher activation energy, with this reflecting an increased difficulty of nickel phase reduction due to a strong interaction between nickel and alumina. The nucleation model, as established using TPR, is successfully validated for the reduction cycle using methane as a fuel gas in a CREC minifluidized riser simulator reactor operating under the expected operating conditions for large industrial scale chemical-looping combustion (CLC) units.

Introduction

During the past few years, chemical-looping combustion (CLC) has received growing attention given its prospective application as an energy efficient CO_2 capture technology for power generation. CLC typically employs a dual fluidized bed system where an oxygen carrier is circulated between two twin beds. The solid carrier thus provides oxygen needed for combustion in the fuel reactor (Figure 1). The oxygen depleted solid material is then transferred to the regenerator to be reoxidized and recycled back to the fuel reactor closing in this manner the CLC "loop". As it can be seen in Figure 1, the separation of fuel and air reactors avoids dilution of flue gas stream with nitrogen. Therefore, the flue gas is constituted primarily by carbon dioxide and water vapor. Condensation of the water vapor allows the separation of carbon dioxide without the need of an extra separation step. Even more given oxygen is supplied in CLC via a solid carrier; this eliminates the need of air. Thus, there is no nitrogen−oxygen contacting in the fuel reactor and as a result no opportunity for nitrogen oxide formation.[1]

Supported metal oxides have been widely studied as suitable oxygen carriers for CLC. Among them alumina supported nickel has received the highest attention given its favorable fluidization properties and thermal stability in a CLC process.[2−12] On the Al_2O_3 support, nickel is present as a dispersed nickel oxide phase. Dispersed phases are less prone to agglomerate when exposed to repeated high temperature CLC cycles.

In an earlier article, we reported a lanthanum modified Ni/La-γAl_2O_3 oxygen carrier suitable for a fluidized bed chemical-looping combustion (CLC) process.[13] Specific surface area analysis showed that the addition of La favors the thermal stability of γAl_2O_3 by preventing phase transformation. The presence of La enhances the reducibility of the oxygen carrier by affecting the metal−support interactions helping the formation of reducible nickel species. Reactive characterization of the prepared oxygen carriers in a CREC (Chemical Reactor Engineering Center) fluidized riser simulator, using multiple reduction/oxidation cycles, demonstrates that the Ni/La-γAl_2O_3 particles display excellent reactivity and stability. The addition of La in the Ni/La-γAl_2O_3 carrier influences the state of the surface minimizing the formation of nickel aluminate. It is argued that the addition of La also inhibits metal particle agglomeration by maintaining consistent metal dispersion during the cyclic oxidation/reduction processes.

The present study focuses on a detailed study of the solid-state reduction kinetics involved using Ni/La-γAl_2O_3 as an

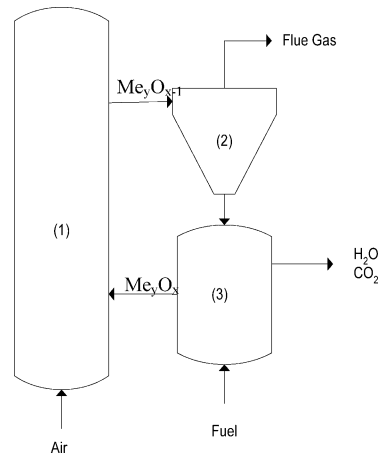

Figure 1. Schematic view of chemical looping combustion: (1) regenerator reactor, (2) cyclone, and (3) fuel reactor.

* To whom correspondence should be addressed. E-mail: hdelasa@eng.uwo.ca.
[†] King Fahd University of Petroleum & Minerals.
[‡] The University of Western Ontario.

10.1021/ie100424w
Published on Web 06/02/2010

oxygen carrier in a CLC process. Regarding the reaction kinetics and in spite of being very critical in determining the fluidized bed unit design and performance, only a very limited number of contributions consider the solid-state kinetics of the reduction/oxidation reactions involved in CLC.[1,4,5,8,14−16]

Gas−solid reaction kinetics becomes more complicated for supported metal/metal oxides materials, given the limited accessibility to the metal/metal oxide, which may depend on both metal and support properties. Thus, even if the physical properties of the particle such as shape and size together with pore size distribution may have an influence, in many cases there may be a dominant support contribution affecting metal−support interactions and orientation of the active components. In the case of a bulk metal oxide, upon reduction, the metal atoms released from the oxide may rapidly agglomerate and sinter forming large metal crystallites. For supported metal oxides however, the metal oxide grains are isolated. Therefore, after reduction the metal atoms must either coalesce with the grain to from small crystallites or migrate over the support to promote the creation of nucleation sites, where crystallite growth occurs.[17] Thus, the following are possible mechanistic steps for the reduction of Ni/Al_2O_3 material using hydrogen as reducing gas: (i) dissociation of hydrogen first on the NiO and then on the surface of Ni^0 clusters as soon they became available, (ii) breaking of Ni−O bonds, to produce more Ni^0 atoms and H_2O molecules (this step can be accelerated or decelerated by foreign cations in the NiO lattice or on the surface), (iii) diffusion of nickel atoms across the support surface away from the center of the reduction, (iv) nucleation of nickel atoms into metallic clusters, after a possible induction period, and (v) crystal growth.[17,18]

Considering the significance of the above-described phenomena, this study addresses the effects of La on the Ni/La-γAl_2O_3 oxygen carrier using various characterization and evaluation catalyst methods. The phenomenological kinetics models considered are established based on physicochemical characterization of a Ni/La-γAl_2O_3 oxygen carrier. The rate-controlling step of the gas−solid reactions is determined by observing the reaction rates at different experimental conditions as well as applying theoretical calculations. Kinetics parameters are established using temperature programmed reduction data. Finally, the developed model is validated using CLC reaction data obtained from a CREC fluidized riser simulator reactor.

Experimental Section

Preparation of La Modified Oxygen Carrier. The solid-state reduction kinetics of the oxygen carriers reported in this article were prepared via an incipient wetness technique. The incipient method offers proper control of metal loading and also provides higher degree of reduction.[4,5] In oxygen carrier preparation, the active metal component nickel was deposited on La modified high surface area (233 m^2/g) γAl_2O_3. The particle size of support γAl_2O_3 was between the 50 and 110 μm ranges. For nickel loading, $Ni(NO_3)_2 \cdot 6H_2O$ was used as a precursor while $La(NO_3)_3 \cdot 6H_2O$ was used to modify the support γAl_2O_3 to improves its thermal stability.

Metal loading (by impregnation), reduction, and calcination are the three main steps involved in oxygen carrier preparation. The samples were prepared with 20 wt % nickel loading which was achieved by a successive impregnation/reduction cycles. In each cycle, 2.5 wt % nickel was added to the support under vacuum condition. The resultant material was left for 1 h under stirring in order to achieve a homogeneous mixture of the nickel nitrate and the support. Following the impregnation step, the resultant paste was then placed into a Thermolyne 48000 furnace for drying by increasing the furnace temperature from ambient to 140 °C over 6 h. The dried solid material was then transferred to a specially designed minifluidized bed reactor located in an oven for reduction. The fluidized bed reactor was connected with a reducing gas mixture containing 10% (by volume) with the balance being helium. During the sample reduction, the bed was first fluidized by supplying the reducing gas mixture. Then, the oven temperature was raised from ambient to 750 °C over 4 h and maintained at 750 °C for 8 h. This thermal treatment under hydrogen flow decomposes $Ni(NO_3)_2$ into NiO, reducing them further into their metallic form. The reaction can be described as follows:

$$Ni(NO_3)_2 + H_2 \rightarrow NiO + 2NO_2 + H_2O$$

$$NiO + H_2 \rightarrow Ni + H_2O$$

$$NO_2 + H_2O \rightarrow HNO_3 + \frac{1}{2}H_2$$

Impregnation, calcinations, and reduction steps were repeated until the desired metal loading (20 wt %) was reached. Once the desired metal loading was attained, the oxygen carrier was calcined in air using the same fluidized bed and the same temperature ramp as used for reduction, i.e., ambient to 750 °C over 4 h and maintained at 750 °C for 8 h. The highest limit (20 wt %) of nickel loading was selected aiming a possible higher amount of oxygen carrying capacity without metal sintering or agglomeration.[4,5]

Temperature Programmed Reduction (TPR). In this investigation, both the characterization of the prepared oxygen carriers and their solid-state reduction kinetics were studied using the temperature programmed reduction data. The hydrogen TPR experiments were conducted at atmospheric pressure using a Micromeritics AutoChem II 2920 analyzer. For each experiment, 100−200 mg of oxygen carrier sample was loaded in a U-shaped quartz reactor tube and placed into the sample port, located inside a heater.

Before each TPR experiment, the oxygen carrier samples were completely oxidized by flowing a stream of gas containing 5% oxygen 95% He at 750 °C. The oxidized sample was then brought back to ambient temperature under Ar flow in order to remove any gas phase oxygen trapped in the oxygen carrier particles. In order to perform the TPR runs, a stream of gas containing 10% H_2 and 90% Ar was circulated through a bed of oxygen carrier particles at a rate of 50 mL/min. At this stage, the temperature program was started to raise the bed temperature from ambient to 950 °C at a prespecified heating rate (10 °C/min). Hydrogen reacted with the oxide(s) with increasing temperature. The gas leaving the reactor was analyzed by using a thermal conductivity dectector (TCD). The TCD signal was further processed to calculate the amount of hydrogen consumed during the reduction process which was used to calculate the number of reducible species (W_{Ni}) and percentage of metal reduction (% reduction) using the following equations:[5]

$$W_{Ni} = \frac{MW_{Ni} V_{H_2} \rho_g}{\upsilon} \quad (1)$$

$$\%\ \text{reduction} = \frac{W_{Ni}}{W_O} \times 100\% \quad (2)$$

H_2 Chemisorption. The hydrogen pulse chemisorption experiments were conducted following each TPR experiments

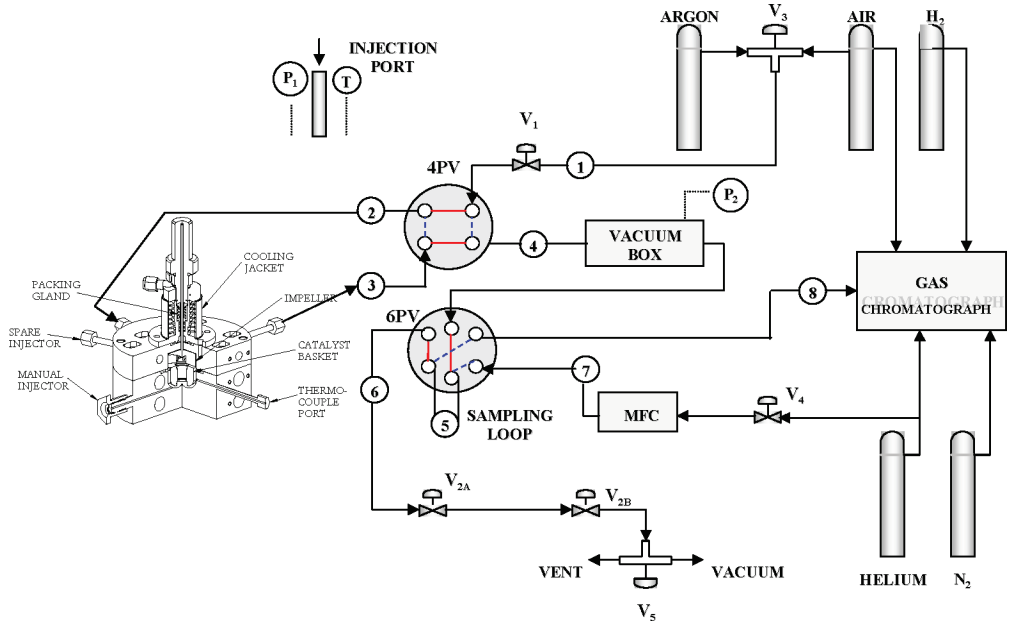

Figure 2. Schematic diagram of the CREC riser simulator (quarter section view) experimental setup (Adapted from ref 19).

as described above using the same Micromeritics AutoChem II 2920 analyzer unit. The chemisorptions data was used to determine percent metal dispersion and active particle size, two very important indicators for establishing a nucleation model described in the modeling section. To perform pulse chemisorption experiment, a series of hydrogen pulses (1.0 mL) were injected into the reduced oxygen carrier sample at ambient temperature. The gas leaving the system was analyzed by a TCD. As hydrogen gas was adsorbed on the metal sites of the reduced oxygen carrier sample, concentration peaks richer in the carrier gas (He) were created. This change in concentration in the outlet stream was recorded by the TCD. When two consecutive peaks had the same area, hydrogen injection was stopped and the peaks were integrated to find the amount hydrogen adsorbed on the metal sites. The percentage of metal dispersion (*% D*) and the average crystallite size (d_v) were calculated form the hydrogen pulse chemisorption using the following relations:[5]

$$\% D = \frac{AX}{Wf} \tag{3}$$

$$d_v = \frac{\varphi V_m}{S_m} \frac{1}{\% D} \tag{4}$$

Kinetics Experiments in the CREC Riser Simulator. In addition to TPR, the solid-state reduction kinetics experiments of the La modified oxygen carriers were established under fluidized bed conditions in a CREC riser simulator and using methane as fuel. The CREC riser simulator is a bench-scale minifluidized bed reactor, invented at CREC-UWO.[19] This 50 cm^3 minifluidized reactor was especially designed for catalyst evaluation and kinetic studies under fluidized bed reactor conditions. A schematic diagram of the CREC riser simulator, along with the gas injector and anemometer location, is illustrated in Figure 2. The detail description of CREC riser simulator can be found elsewhere.[13,19]

For each experiment in the CREC riser simulator, 0.5−1 g of oxygen carrier was first loaded into the reactor and the system was then flashed by flowing argon. The reactor was then brought to the desired temperature ranging between 550 and 680 °C under argon flow by using a temperature programmed ramp of 10 °C/min. The argon flow was stopped once the reactor reached the desired temperature and the vacuum box pressure was brought to 20.7 kPa (3.0 psi) using a vacuum pump. At this stage, the impeller was turned on and the methane (10 mL) was injected into the reactor using a preloaded syringe. The reaction was allowed to take place for prespecified reaction times varied between 10 and 60 s. This reaction time was defined from the instant methane was fed to the CREC riser simulator unit to the time the valve isolating the reactor and the vacuum bottle was opened and the contents of the reactor were evacuated to the vacuum bottle. Finally, the product species were analyzed using a gas chromatograph. Before the next cycle, the oxygen carrier was regenerated (oxidized) by flowing air.

Results and Discussions

Reducibility, Metal Dispersion, and Metal Crystallite Size. In the context of the present study, the TPR characterizations were carried out in order to determine the temperature range in which the oxygen of the carrier will react with the gas phase reducing agent (in this case hydrogen). The TPR profile analysis allowed indentifying the reducible species of the metal oxides in the studied temperature range. TPR also facilitated the assessment of the effects of La on the oxygen carrier reducibility under repeated reduction/oxidation cycles and any possible losses in oxygen carrier activity as a result of metal−support interactions yielding nonreducible species and nickel crystallite agglomeration. All of this information was very crucial in model development and evaluation.

Figure 3 shows a TPR profile of a La modified Ni/La-γAl_2O_3 oxygen carrier obtained from an experiment of ambient to 950 °C temperature range with 10 °C/min increment. As it can be seen from the figure, the reduction profile of the La modified sample displays a single, symmetric, and comparatively narrow peak at 580 °C. In addition to that, a very small peak was also appeared at 850 °C. The first peak is assigned to the reduction of the dominant metal phase, mainly NiO, while the second peak is due to the reduction of a small amount of nickel aluminate. For a similar alumina supported nickel catalyst studied, Richardson et al. suggested that NiO and $NiAl_2O_4$ are

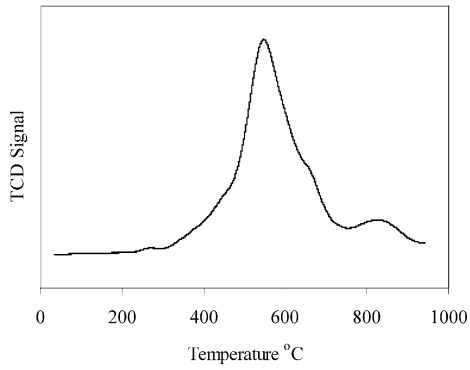

Figure 3. TPR profile of a Ni/La-γAl_2O_3 sample: heating rate 10 °C/min; reducing agent 10 mol % H_2, balanced Ar at 50 cm^3/min.

reducible phases in the 325−700 °C range, with the species being reduced above 600 °C into nickel aluminate.[20]

XRD analysis of the La promoted samples (reported in Hossain et al.) also identified NiO and $NiAl_2O_4$ phases on both the Ni/γAl_2O_3 and Ni/La-γAl_2O_3 samples, with no lanthanum-containing phase detected.[13] This observation further confirms that La, in addition to providing thermal stability γAl_2O_3, also helps to enhance the reducibility of Ni species, not being included in the metallic crystalline phase. Jin et al. investigated Ni on Al_2O_3 oxygen carriers suitable for CLC reporting the formation of $NiAl_2O_4$ using XRD analysis of the oxidized sample.[8] According to Jin et al., $NiAl_2O_4$ is very difficult to reduce and even the phase stable up to 900 °C.

As mentioned in the experimental section, hydrogen pulse chemisorption was conducted after each cycle of reduction of the oxygen carrier sample. The metal dispersion and the crystallite size determined by the pulse chemisorption experiments confirmed the stable behavior of the prepared samples during consecutive reduction and oxidation cycles (Figure 4). One can clearly observe in Figure 4 that although both unmodified and modified samples provide stable metal dispersions a higher metal dispersion was observed in the La modified carrier: 0.9% and 2.5% for the unpromoted support and La promoted respectively. Thus, it appears that addition of La alters the γAl_2O_3 support surface in such a way that the degree of interaction between Ni crystallites and the La-γAl_2O_3 helps as well to maintain a consistent metal dispersion during successive oxidations and reductions. The consistent crystallite size of the reduced sample was further confirms the positive effects of La on the nickel dispersion on La-γAl_2O_3. H_2 chemisorption suggests that metal crystallite sizes remain almost constant over repeated redox cycles, with this being a good indicator of the nearly absent metal sintering. Even more, the relatively high and stable metallic surface area of the La modified promoted carrier further confirms the uniform and unchanged metal crystallite sizes obtained in previous studies.[13]

Kinetics Modeling. Steps Involved. The fuel reactor of a CLC process involves the combustion of gas phase fuel with the solid phase metal oxide resulting the reduction of oxygen carrier. It is considered that the reduction of the oxygen carrier in the fuel reactor proceeds through different steps according to the following sequence:[14] transfer of gas phase fuel from the bulk gas stream to the outer surface of the oxygen carrier, diffusion trough the porous structure, and then through a solid ash layer within each grain, and finally reaction between the fuel and the solid phase oxygen. The combustion gas thus generated diffuses back between the reduced metal crystallites and, finally, through the bulk gas phase boundary layer surrounding the oxygen carrier. The above-described steps in a

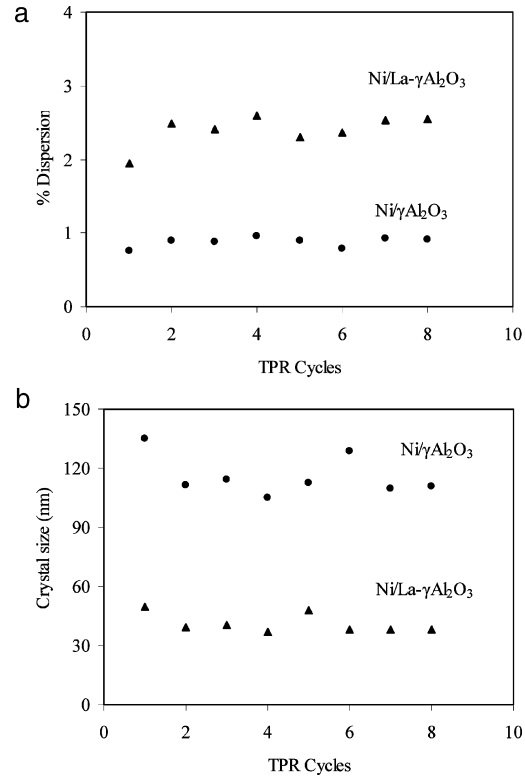

Figure 4. (a) Metal dispersion and (b) crystallite size during the repeated TPR cycles.

fuel reactor have their own kinetics that can limit or influence the overall rate of the reaction. Depending on the reaction conditions and oxygen carrier size, the resistances in one of the above-mentioned steps can vary significantly and only the highest resistance must be considered as the rate-limiting step.

Like heterogeneous catalytic reactions, the rate-controlling steps of the gas−solid reaction involved in a fuel reactor can be determined by conducting reactions at a well selected set of reaction conditions. In order to model the overall kinetics as an intrinsic reaction rate, the transport resistances must be eliminated.

The bulk diffusion resistance mainly depends on the particle size of the oxygen carrier, the gas phase velocity between a solid particle and gas properties. In this investigation, the kinetics TPR experiments were carried out in a packed bed of 50−110 μm size particles. The experimental parameters were set such that the reaction system could be modeled as a differential reactor and were assessed using the Sherwood number along with Froessling's correlations.[21,22]

$$Sh = 2 + 1.1Sc^{0.33}Re^{0.6} \tag{5}$$

$$k_{mc} = \frac{ShD_{AB}}{d_p} \tag{6}$$

and

$$(C_{Ag} - C_{As})_{film} = \Delta C_{film} = \frac{(-r'_{A(obs)})}{k_{mc}a_p} \tag{7}$$

The TPR reaction experiments were evaluated at the worst possible conditions, assuming stagnant fluid condition i.e., the lowest value of *Sh* equals 2. This lowest value corresponds to the highest possible gas film resistances. The calculated value of ΔC_{film} was found to be 0.00005 mmol/m^3 indicating a

negligible concentration gradient of the gas phase reactant in the bulk phase to the oxygen carrier outer surface.

The internal diffusion was assessed using the Weisz−Prater criterion, which suggests that internal mass transfer resistance is negligible if the following inequality is satisfied.[22]

$$C_{WP} = \frac{-r'_{A(obs)}\rho_P {R_P}^2}{D_{eff}C_{AS}} \ll 1 \tag{8}$$

In the context of the present study the C_{WP} dimensionless parameter value was found to be 0.00009 for reduction with this confirming the negligible influence of intraparticle diffusion.

Model Formulations. As observed above, the reduction of the oxygen carrier reactions in TPR were free from both external and internal transport limitations. Consequently, the solid-state reduction process of the oxygen carrier of this study can be formulated considering an overall reaction rate being a function of the degree of reduction of the solid material $f(X_P)$ and the composition of the species in the gas phase.[4,14,23,24]

$$\frac{dX_P}{dt} = k(T)f(X_P)f(p_A, p_B) \tag{9}$$

where, X_P is the progress of the oxygen carrier reduction, while p_A and p_B represent the partial pressure of the reactant and products, respectively.

For the TPR data, the degree of reduction of the oxygen carriers can be defined using hydrogen consumption data according to the following relation:

$$X_P = \frac{\Delta n_t}{\Delta n_{total}} \tag{10}$$

where Δn_t represents the moles of hydrogen or moles of oxygen consumed at time t (min) and Δn_{total} represents the total moles of hydrogen consumed for the complete reduction of the oxygen carrier sample.

In the context of the present study, the function $f(p_{A_2}, p_B)$ of eq 9 was lumped into a single pseudoconstant given that all the TPR experiments were carried out at the same feed flow rate and hydrogen partial pressure. The effect of water was neglected for TPR differential conversions experiments.

Nucleation and Nuclei Growth Model. According to the nucleation and nuclei growth model, the reduction of the oxygen carrier material proceed by nuclei formation and subsequent nuclei growth. Nucleation of the active sites is a dynamic process, which practically initiates the reaction. The reduction reaction is then progress with both nucleation and growth of the already formed nuclei. The growth of the formed nuclei might occur due to the overlap of the nuclei and/or ingestion of a nuclei site. Therefore, the overall conversion of the oxygen carrier reduction should be determined by the relative rate of nucleation, nuclei growth, and the concentration of the potential nucleus-forming sites. For a given temperature and gas phase composition, the nuclei growth rate is constant. The possible steps during a gas−solid reaction following the nucleation and nuclei growth model can be found in studies by Sedor et al. and Hossain and de Lasa.[6,14] According to the nucleation and nuclei growth model, the reduction oxygen carrier proceeds through nucleation and possible crystal growth with this leading to the following equation.[4,24,25]

$$f(X_P) = n(1 - X_P)[-\ln(1 - X_P)]^{(n-1)/n} \tag{11}$$

where, n is the Avrami exponent indicative of the reaction mechanism and crystal growth dimension.

Under these assumptions, substituting eq 11 and the Arrhenius equation into the fundamental kinetic equation eq 9 yields

$$\frac{dX_P}{dt} = nk_0 \exp\left[\frac{-E_{app}}{R}\left(\frac{1}{T} - \frac{1}{T_m}\right)\right](1 - X_P)[-\ln(1 - X_P)]^{(n-1)/n} \tag{12}$$

where E_{app} can be interpreted as the difference between the activation energy for growth and the activation energy for nucleation.[4]

Unreacted Shrinking-Core Model. According to the unreacted shrinking-core model the reduction of a supported metal oxide oxygen carrier progresses by[14]

$$C_{NiO,0}W_{OC}\frac{dX_P}{dt} = br_m \tag{13}$$

where, r_m is the rate of reaction per unit mass of the oxygen carrier. Given the reaction is controlled by the chemical process, the reaction rate per unit mass in the balance equation can be directly related to the reaction per unit surface area of the solid particles:

$$r_m = a_0 S(X_P) r_s \tag{14}$$

where, a_0 is the initial specific surface area of oxygen carrier, r_s is the specific surface reaction rate, and $S(\alpha)$ reflects the change in the area of the reaction surface as a function of particle conversion. This function depends on the structure of the oxygen carrier particles.

Combining eqs 13 and 14 yields

$$\frac{dX_P}{dt} = \frac{a_0 b}{C_{NiO,0}W_{OC}} S(X_P) r_s \tag{15}$$

According to the shrinking-core spherical grain model the particle conversion is obtained from the changing volume of the particle:

$$X_P = 1 - \frac{\text{volume of unreacted core}}{\text{volume of total particle}} = 1 - \left(\frac{r_{OC}}{R_{OC}}\right)^3 \tag{16}$$

therefore, the function $S(X_P)$ (in eq 15) can be expressed as

$$a_0 S(X_P) = 4\pi {R_{OC}}^2 (1 - X_P)^{2/3} \tag{17}$$

The surface reaction rate (r_s) can be formulated considering the reaction between the gas phase methane and solid NiO phase is the sole heterogeneous reaction taking place, as already seen in TPR analysis.

Furthermore, earlier studies suggested that the alumina supported NiO reduction proceeds through adsorption of reducing gas (H_2 in this case) on the NiO sites, as sites become available followed by the rupture of Ni−O bonds to produce the metallic Ni, CO_2, and H_2O.[26,27] In such models both adsorption and desorption processes are considered faster steps than the surface reaction. Thus, considering a first-order reaction with respect to methane, the surface reaction rate can be formulated as

$$r_s = k_s C_{H_2} = k_s(1 - aX_P) \tag{18}$$

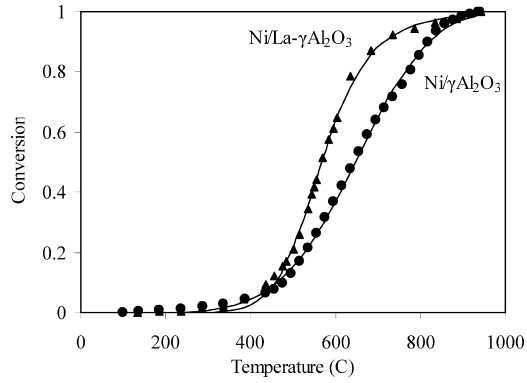

Figure 5. Conversion plots for nonisothermal reduction: (i) Ni/γAl_2O_3 and (ii) Ni/La-γAl_2O_3 samples (the solid lines are the model predicted values) (Note: Reported points are one every 2 min to avoid overcrowding the figure. The original data file includes data points taken every 2 s).

Substituting eq 17 and 18 into eq 15 and for the Arrhenius equation yields

$$\frac{dX_P}{dt} = k_0 \exp\left[\frac{-E}{R}\left(\frac{1}{T} - \frac{1}{T_0}\right)\right](1 - X_P)^{2/3}(1 - aX_P) \tag{19}$$

where, $k_0 = [(a_0 b)/(C_{NiO,0} W_{OC})]k_{s0}$ and E is the energy of activation energy for the reduction of solid oxygen carrier.

Parameters Estimation and Model Discrimination. The applicability of the kinetic models described in the previous section was investigated in the present study using the temperature programmed reduction (TPR) data. For kinetics analysis, the rate of oxygen carrier reduction were explicitly related to the rate of consumption of the hydrogen during the TPR experiments. The reduction rate maxima occurred between 60−70% conversion levels. The TPR experiments were highly reproducible with reduction maxima temperature within ±5 °C.

A least-squares fitting of the k_0, E_{app}, and n parameters of eq 12 and 19 was implemented using MATLAB. The data points for the evaluation of these three parameters were obtained using more than 150 data points (data taken one every two minutes). Thus, the degree of freedom for the model was over 150−3 = 147 with this showing the abundant experimental data available to adjust the model parameters. Discrimination between models was based on the correlation coefficient (R^2), lower residual SSQ, smaller individual confidence intervals for model parameters and minimum cross-correlation coefficients. Given the R^2 values and spans of the parameters obtained, it was concluded that with the nucleation and nuclei growth model better fitting is achieved using an n value close to one. Thus, random nucleation ("n" value of 1) was selected as best, and a close to constant crystallite size hypothesized, during repeated reduction and oxidation cycles. Moreover, at higher values of n, for instance $n = 2$, the R^2 values were 0.7 instead of 0.99 and the spans were increased from 5−10% to 30−40%. All this was considered an indication of the very limited crystallite growth between cycles. Even more when random nucleation and the shrinking core models were compared; still the random nucleation model was favored and this considers the higher R^2 and lower SSQ values.

Figure 5 shows the comparison between the experimental and nucleation model (for $n = 1$) predicted conversions during reduction of the oxygen carrier samples. One can notice that when data points are compared with model predictions that there is a normal distribution of residuals with high correlation coefficients.

Table 1. Estimated Model Parameters for TPR Cycles Using the Nucleation Model[a]

sample ID	E (kJ/mol)	$k_0 \times 10^4$	R^2	γ^{*b}
Ni/γAl_2O_3	104.5 ± 3	16 ± 1.5	0.99	0.61
Ni/La(1)-γAl_2O_3	75.3 ± 2.4	12 ± 1.8	0.98	0.68
Ni/La(5)-γAl_2O_3	73.4 ± 2.6	21 ± 1.1	0.99	0.59

[a] Repeats displayed a typical ±3.4% standard deviation. [b] Cross--correlation coefficient.

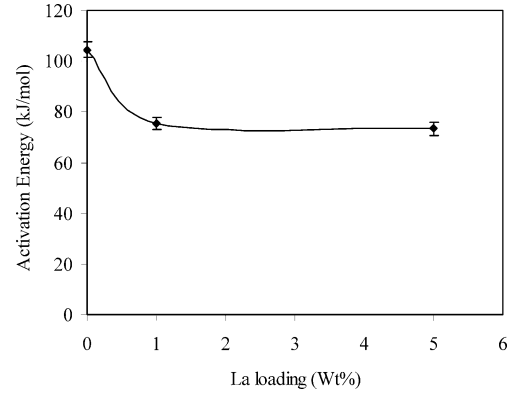

Figure 6. Activation energy for reduction of Ni/La-γAl_2O_3 sample at different La loading.

Another interesting observation is that the activation energy for the reduction of the Ni/La-γAl_2O_3 oxygen carrier obtained varies between 70 and 105 kJ/mol, which is within the range (17−135 kJ/mol) reported by many researchers.[27] According to these studies, the activation energy falls into three groups depending on the reduction rate-controlling regime. A first group exhibiting low activation energy (15−25 kJ/mol) points toward the external or very strong pore diffusion resistance limiting the overall reaction. A second group with activation energies of 40−50 kJ/mol indicates the pore diffusion controlling the overall reduction reaction. Finally a third group, with activation energy in the 65−135 kJ/mol range shows the chemically reaction controlled reduction.

One should notice that the reduction activation energy (Table 1) estimated from the nucleation model falls within the chemically reaction controlled region values which is consistent with the hypothesized absence of internal or external mass transport limitations.

Figure 6 displays the estimated activation energies of the La modified Ni/La-γAl_2O_3 oxygen carriers at different La loadings. After an initial decrease, the activation energy remained almost unchanged with the increase of La loading. This observation suggests that small amounts of La are enough to modify the oxygen carrier with minimization of the interaction between Ni and alumina.

Model Evaluation using CREC Riser Simulator Data. While the TPR data are of significant value for evaluating kinetic models, one has to be very cautions in terms of extending these kinetic models, developed in fixed bed reactors, to fluidized bed processes where fluid dynamic patterns, concentration profiles, and oxygen carrier contacting history will vary significantly. With this end, experiments were developed in a CREC riser simulator for confirmation of the applicability of the established heterogeneous reduction model using methane as the reducing agent.

As mentioned in the experimental section, this reactor operates in batch reactor mode under turbulent fluidized bed reactor conditions. Therefore, it allows generating conversion data for different reaction times, which is essential to estimate

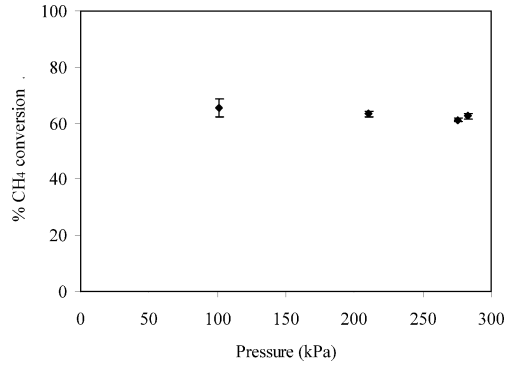

Figure 7. Effect of total pressure on methane conversion in the CREC riser simulator: T 650 °C; $W_{carrier}$ 0.5 g; V_{CH4} inj. 10 mL.

the kinetics parameters in the differential equation (eq 12) describing the reduction kinetics of the solid particles. Methane and nickel oxide conversions are two important parameters required to evaluate the model(s) defined as follows:

(i) Methane conversion is calculated from the product analysis data using eq 20, since CO_2 is the only carbon-bearing component in the methane combustion product[13]

$$X_{CH_4} = \frac{C_{CO_2,out}}{C_{CH_4out} + C_{CO_2,out}} \times 100\% \qquad (20)$$

These concentrations of methane and carbon dioxide in the reactor are determined through gas chromatography of the product gases.

(ii) Nickel oxide(s) conversion is calculated on the basis of the number of moles of reacted oxygen, the weight of the carrier, and the nickel composition of the carrier.

Nickel oxide conversion was then calculated:

$$X_{NiO} = \frac{4N_{CH_40}X_{CH_4}}{\left(\frac{wX_{W,NiO}}{MW_{NiO}}\right)} \times 100\% \qquad (21)$$

where, N_{CH40} is the initial number of moles of methane injected into the CREC riser reactor or the moles of methane into the CREC riser reactor at reaction time zero, X_{CH4} is the conversion of methane, w is the mass of oxygen carrier loaded into the reactor, $X_{W,NiO}$ is fraction of nickel oxide present in the oxygen carrier sample and MW_{NiO} is the molecular weight of nickel oxide.

To determine the kinetic parameters of eq 12, experiments were conducted at different temperature levels between 550 and 680 °C and at close to atmospheric pressure (1.05−1.1 atm). Preliminary experiments in the CREC riser simulator indicated negligible effects of total pressure on the conversion, as shown in Figure 7. Therefore, all the experiments in this investigation were conducted at closed to atmospheric pressure.

The conversion data in the CREC riser simulator as a function of temperature is reported in Figure 8. It is apparent from this data that the temperature has a strong influence on the reduction rate of the oxygen carrier particles, especially at the lower temperature levels. Reduction tests below 550 °C show that the reduction rate is very slow indicating a possible "incubation" period before the reduction reaction begins in earnest. Data collected from 550 to 650 °C also show that the oxide carrier conversion steeply increases at this higher temperatures range. Even more while approximately 80% conversion was achieved

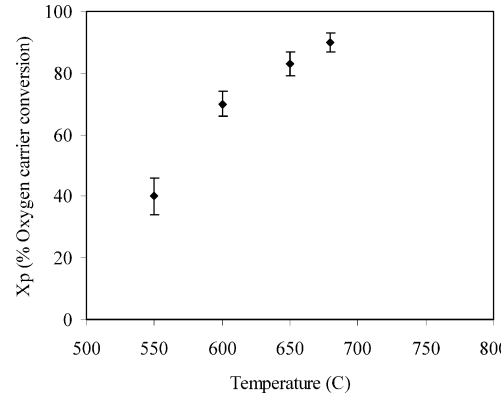

Figure 8. Conversion of oxygen carrier in the CREC riser simulator at different temperatures: CH_4 as fuel, contact time 40 s; P 1 atm; $W_{carrier}$ 0.5 g; V_{CH4} inj. 10 mL.

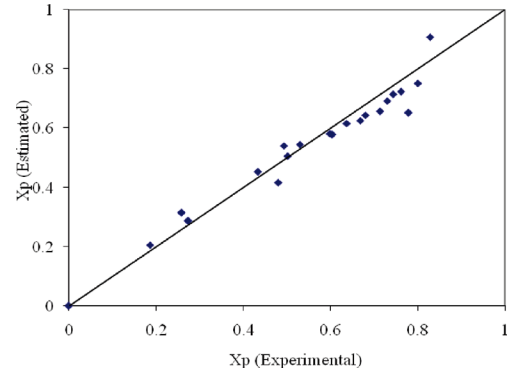

Figure 9. Experimental data obtained using the CREC riser simulator and fitted nucleation and nuclei growth model: CH_4 as fuel, T 550−680 °C; P 1 atm; $W_{carrier}$ 0.5 g; V_{CH4} inj. 10 mL.

Table 2. Comparison of Estimated Parameters for the Reduction of Ni/La(5)-γAl_2O_3 Oxygen Carrier using TPR and CREC Riser Simulator Data

data	fuel	E (kJ/mol)	$k_0 \times 10^4$	R^2	γ^{*a}
TPR data	H_2	73.4 ± 2.6	21 ± 1.1	0.99	0.59
CREC riser simulator data	CH_4	69.3 ± 10.1	44.1 ± 28.4	0.96	0.65

[a] Cross-correlation coefficient.

in a 40-s reaction time at 650 °C, oxygen carrier conversion reaches the 90% level at 680 °C.

For model validation for the isothermal conversion data collected at the set temperatures in the 550−680 °C range, various reaction times (20−60 s) were considered. As well, kinetic parameters were introduced into the nucleation and nuclei growth model (eq 12). This differential equation was solved to predict particle conversions for different reaction times and temperatures. Kinetic parameters were regressed until good fitting between experimental and simulated conversion were obtained. One should notice the adequate kinetic parameter determination with the following statistical indicators: (i) degree of freedom 21 − 2 = 19, (ii) parameter span for the 95% confidence interval 15%, (iii) regression coefficient 0.96.

Figure 9 compares the experimental and model predicted particle conversions. It is interesting to see that the nucleation and nuclei growth model with $n = 1$ fits the experimental data adequately. Table 2 presents as well a comparison of the estimated energy of activation for the reduction of NiO/La-γAl_2O_3 oxygen carrier using TPR and the CREC riser simulator.

It is encouraging to see the consistency of the energy of activations obtained using these two different experimental

setups: TPR and CREC fluidized riser simulator. As a result, one can conclude the ability of the CREC fluidized simulator to establish both a kinetic model and kinetic parameters under the expected operating conditions of industrial scale fluidized CLC units.

Conclusions

The characterization and kinetic study of both the La modified Ni/La-γAl_2O_3 and Ni/La-γAl_2O_3 oxygen carrier sample reveal the following:

(i) TPR results indicated that the modification of alumina with La helps increase the reducibility of the oxygen carrier by formation of NiO and minimization of the formation of $NiAl_2O_4$.

(ii) H_2 chemisorption demonstrates that La can offer better nickel dispersion/redispersion on alumina support. It is hypothesized that La interacts more readily with the alumina support, inhibiting the nickel aluminate formation.

(iii)The nucleation and nuclei growth model with random nucleation mechanism ($n = 1$) is found to describe the experimental data adequately, with various parameters being determined with their appropriate statistical spans for good fitting.

(iv)The activation energies for Ni/La-γAl_2O_3 reduction is found to be in the 73 kJ/mol level significantly lower than the 105 kJ/mol activation energies for the unprompted Ni/γAl_2O_3 reduction.

(v) The favorable effect of La reducing the activation energy of La modified oxygen carrier reducibility is consistently confirmed both in the TPR unit and the CREC fluidized riser simulator.

Acknowledgment

The authors would like to thank Natural Science and Engineering Research Council (NSERC) of Canada for financial support to this project. The authors would also like to gratefully acknowledge the support of King Fahd University of Petroleum and Minerals, Saudi Arabia, for his financial support of M.M.H.

Notation

A = constant
a_0 = initial specific surface area of oxygen carrier (m^2/g)
a_p = external surface area of the oxygen carrier (cm^2/g)
b = stoichiometirc coefficient of the solid phase reactant
C_{Ag} = bulk concentration of gaseous reactant (mol/cm^3)
C_{As} = surface concentration of gaseous reactant (mol/cm^3)
$C_{NiO,0}$ = initial molar concentration of NiO/Ni in the oxygen carrier (mol/g)
D_{AB} = molecular diffusivity (cm^2/s)
D_{eff} = effective diffusivity (cm^2/s)
d_p = particle diameter (cm)
E_{app} = apparent activation energy for oxidation/reduction (kJ/mol)
f = fraction of reduced metal
k = specific rate of the overall reaction (mol/s)
k_{mc} = external mass transfer coefficient (cm/s)
N = number of nickel crystals of d_{pi} size
n = dimensions of the growing crystals
p_i = partial pressure of the gas phase reactant i (kPa)
Re = Reynolds number
R_p = particle radius (cm)
r_m = reaction rate per unit mass of the oxygen carrier (mol/g)
$-r'_{A(obs)}$ = observed reaction rate (mol/g)
r_s = specific surface reaction rate ($mol/m^2 \cdot s$)
S = surface area as a function of particle conversion (m^2/g)
Sc = Schmidt number
Sh = Sherwood number
S_m = average surface area of metal particles exposed (m^2/g)
T_m = centering temperature (K)
V_{H2} = volume of hydrogen consumed at STP
V_m = volume of metal atoms (cm^3)
W = percentage of weight metal
W_{OC} = weight of the oxygen carrier (g)
W_{Ni} = weight of reducible species
MW_{Ni} = molecular weight of reducible species
X = total hydrogen chemisorbed
X_{CH4} = conversion of methane
X_P = degree of conversion of oxygen carrier
α_{total} = extended degree of conversion of the oxygen carrier
β = rate of temperature increase (K/min)
ρ_g = gas molar density at STP (mol/m^3)
ρ_p = particle density (g/cm^3)
φ = particle shape constant
υ = stoichiometric coefficient

Literature Cited

(1) Ishida, M.; Jin, H. A novel chemical-looping combustor without NO_x formation. *Ind. Eng. Chem. Res.* **1996**, *35*, 2469.

(2) Hossain, M. M.; de Lasa, H. I. Chemical-looping combustion (CLC) for inherent CO_2 separation - a review. *Chem. Eng. Sci.* **2008**, *63*, 4433.

(3) Hossain, M. M.; Sedor, K. E.; de Lasa, H. I. Co-Ni/Al_2O_3 oxygen carrier for fluidized bed chemical-looping combustion: desorption kinetics and metal-support interaction. *Chem. Eng. Sci.* **2007**, *62*, 5464.

(4) Hossain, M. M.; de Lasa, H. I. Reactivity and stability of Co-Ni/Al_2O_3 oxygen carrier in multicycle CLC. *AIChE J.* **2007**, *53*, 1817.

(5) Sedor, K. E.; Hossain, M. M.; de Lasa, H. I. Reactivity and stability of Ni/Al_2O_3 oxygen carrier for chemical-looping combustion (CLC). *Chem. Eng. Sci.* **2008**, *63*, 11–2994.

(6) Sedor, K. E.; Hossain, M. M.; de Lasa, H. I. Reduction kinetics of a fluidizable nickel-alumina oxygen carrier for chemical-looping combustion. *Can. J. Chem. Eng.* **2008**, *86*, 323.

(7) Adanez, J.; de Diego, L. F.; Garcia-Labiano, F.; Gayan, P.; Abad, A. Selection of oxygen carriers for chemical-looping combustion. *Energy Fuels* **2004**, *18*, 371.

(8) Jin, H.; Okamoto, T.; Ishida, M. Development of novel chemical-looping combustion: Synthesis of solid looping material of Ni/$NiAl_2O_4$. *Ind. Eng. Chem. Res.* **1999**, *38*, 126.

(9) Mattisson, T.; Johansson, M.; Lyngfelt, A. Reactivity of some metal oxides supported on alumina with alternating and oxygen-Application of chemical-looping combustion. *Energy Fuel* **2003**, *17*, 643.

(10) Son, S. R.; Kim, S. D. Chemical-looping combustion with NiO and Fe_2O_3 in a thermobalance and circulating fluidized bed rector with double loops. *Ind. Eng. Chem. Res.* **2006**, *45*, 2689.

(11) Garcia-Labiano, F.; Adanez, J.; de Diego, L. F.; Gayan, P.; Abad, A. Effect of pressure on the behavior of copper-, iron-, and nickel-based oxygen carrier for chemical-looping combustion. *Energy Fuel* **2006**, *20*, 26.

(12) Cho, P.; Mattisson, T.; Lyngfelt, A. Defluidization conditions for a fluidized bed of iron oxide-, nickel oxide-, and manganese oxide-containing oxygen carriers for chemical-looping combustion. *Ind. Eng. Chem. Res.* **2006**, *45*, 968.

(13) Hossain, M. M.; Lopez, D.; Herrera, J.; de Lasa, H. I. Nickel on lanthanum modified γ-Al_2O_3 oxygen carrier for CLC: Reactivity and stability. *Catal. Today* **2009**, *143*, 179.

(14) Hossain, M. M.; de Lasa, H. I. Reduction and oxidation kinetics of Co-Ni/Al_2O_3 oxygen carrier involved in a chemical looping combustion process. *Chem. Eng. Sci.* **2010**, *65*, 98.

(15) Abad, A.; Adanez, J.; Gracia-Labiano, F.; de Diego, L. F.; Gayan, P.; Celaya, J. Mapping of the range of operational conditions for Cu-, Fe-, and Ni-based oxygen carriers in chemical-looping combustion. *Chem. Eng. Sci.* **2007**, *62*, 533.

(16) Ryu, H.-J.; Bae, D.-H.; Han, K.-H.; Lee, S.-Y.; Jin, G.-T.; Choi, J-.H. Oxidation and reduction characteristics of oxygen carrier particles and reaction kinetics by unreacted core model. *K. J. Chem. Eng.* **2001**, *18*, 831.

(17) Richardson, J. T.; Scates, R. M.; Twigg, M. V. X-ray diffraction of hydrogen reduction of NiO/α-Al_2O_3 steam reforming catalysts. *Appl. Catal. A: Gen.* **2004**, *267*, 35.

(18) Gavalas, G. R.; Phichitkul, C.; Voecks, G. E. Structure and activity of NiO/α-Al_2O_3 and NiO/ZrO_2 calcined at high temperatures. I. structure. *J. Catal.* **1984**, *88*, 54.

(19) de Lasa, H. I. *Riser simulator for catalytic cracking studies*. US Patent 5,102,628, 1992.

(20) Richardson, J. T.; Turk, B.; Twigg, M. V. Reduction of model steam reforming catalysts: effect of oxide additives. *Appl. Catal. A: Gen.* **1996**, *148*, 97.

(21) Heynderickx, G. J.; Schools, E. M.; Marin, G. B. Coke combustion and gasification kinetics in ethane steam crackers. *AIChE J.* **2005**, *51*, 1415.

(22) Fogler, H. S. *Element of Chemical Reaction Engineering*, 3rd ed.; Prentice Hall Int. Inc.: New York, 1999.

(23) Kanervo, J. M.; Krause, A. O. I. Characterization of supported chromium oxide catalysts by kinetics analysis of H_2-TPR data. *J. Catal.* **2002**, *207*, 57.

(24) Kanervo, J. M.; Krause, A. O. I. Kinetics analysis of temperature-programmed reduction: Behavior of a CrO_x/Al_2O_3 catalyst. *J. Phy. Chem. B* **2001**, *105*, 9778.

(25) Brown, M. E. *Introduction to thermal analysis: Techniques and applications*, 2nd ed.; Kluwer Academic Publishers: Dordrecht, The Netherlands, 2001.

(26) Bandrowski, J.; Bickling, C. R.; Yang, K. H.; Hougen, O. A. Kinetics of nickel oxide by hydrogen. *Chem. Eng. Sci.* **1962**, *17*, 379.

(27) Richardson, J. T.; Scates, R. M.; Twigg, M. V. X-ray diffraction of nickel oxide reduction by hydrogen. *Appl. Catal. A: Gen.* **2003**, *246*, 137.

Received for review February 25, 2010
Revised manuscript received April 19, 2010
Accepted April 23, 2010

IE100424W